Applied Microscopy
Korean Society of Microscopy

pISSN 2287-5123 · eISSN 2287-4445
http://dx.doi.org/10.9729/AM.2012.42.3.158

Precise Comparison of Two-dimensional Dopant Profiles Measured by Low-voltage Scanning Electron Microscopy and Electron Holography Techniques

Moon Seop Hyun[1,2], Jung Ho Yoo[1], Noh-Yeal Kwak[3], Won Kim[3], Choong Kyun Rhee[2,4], Jun-Mo Yang[1,*]

[1]Measurement & Analysis Team, National Nanofab Center, Daejeon 305-806, Korea
[2]Department of Chemistry, Chungnam National University, Daejeon 305-704, Korea
[3]R & D Division, SK Hynix Inc., Icheon 467-701, Korea
[4]Graduate School of Analytical Science and Technology, Chungnam National University, Daejeon 305-704, Korea

*Correspondence to:
Yang JM,
Tel: +82-42-879-9550
Fax: +82-42-879-9609
E-mail: jmyang@nnfc.re.kr

Received September 2, 2012
Revised September 7, 2012
Accepted September 10, 2012

Detailed comparison of low-voltage scanning electron microscopy and electron holography techniques for two-dimensional (2D) dopant profiling was carried out with using the same multilayered *p-n* junction specimen. The dopant profiles obtained from two methods are in good agreement with each other. It demonstrates that reliability of dopant profile measurement can be increased through precise comparison of 2D profiles obtained from various microscopic techniques.

Key Words: 2-dimensional dopant profiling, *p-n* junction, Electron holography, Low-voltage scanning electron microscopy

INTRODUCTION

As the size of metal-oxide-semiconductor field-effect transistors (MOSFETs) shrinks to nanoscale, the precise and reliable dopant profiling in shallow junctions has become important for device modeling and operation (Bertrand et al.,2004). Secondary ion mass spectrometry (SIMS) and spreading resistance profiling are widely used as practical characterization techniques to reveal one-dimensional (1D) dopant distribution in *p-n* junctions. However, both techniques are not sufficient to delineate the accurate and reliable lateral dopant distribution of nanoscaled MOSFETs devices. Two-dimensional (2D) dopant profiling methods such as chemical etching delineation (CED) (Eo et al., 2004; Shaislamov et al., 2008), scanning capacitance microscopy (SCM) (Zavyalov et al., 1999; Morita, 2007), electron holography (EH) (Völkl et al., 1998; Tonomura, 1999), and low-voltage scanning electron microscopy (LV-SEM) (Venables & Maher, 1996; Elliott et al., 2002; El-Gomati et al., 2005) have been received a lot of attention due to their high spatial resolution.

The CED method is based on the chemical etching of the specimen containing *p-n* junctions, where etching rate depends on the difference of dopant type and concentrations. This method is favored due to its quick and simple experimental procedure. However, due to the difficulty in controlling the etching process, this technique does not provide reproducibility and quantitative information. On the other hand, the SCM technique which is based on the atomic force microscope has been shown to be useful for the quantitative 2D dopant profiling with good sensitivity and wide dynamic range of 10^{15}~10^{20} atom/cm^3. This technique can extract the 2D carrier profiles in semiconductor devices by mapping the local capacitance variation (dC/dV) between

This work was supported by "Development Program of Nano Process Equipments" of Korea Ministry of Knowledge Economy [Project No. 10034790, Development of LP-CVD System for Boron Doped Silicon].

a metallic tip and a sample. One of the drawbacks of SCM is that the capacitance variation and the *p-n* junction line are considerably affected by the thickness and quality of the surface oxide layer and the electrical property of the tip.

EH is also very promising in terms of possibility to provide quantitative information and high spatial resolution. Since EH is based on transmission electron microscopy (TEM), very high resolution can be achieved. It was reported that the potential resolution for dopant profiling is around 0.1 V across the *p-n* junction (Rau et al., 1999). Recently, dopant contrasts in SEM can be achieved at a low accelerating voltage range with incident beam energies of ~1 keV, which is called the LV-SEM technique. Even though phenomenon of dopant contrast in SEM was first reported in 1967, this method has not been widely studied due to the low performance of the early SEMs at the low accelerating voltage. However, as a recent SEM instrumentation has been improved with the spatial resolution of 1 nm level, LV-SEM has attracted much attention as a potential technique for easy, quick and reliable 2D dopant profile measurement over a wide area, especially in real devices. Each doped region in LV-SEM can be clearly visualized with bright (*p*-type) and dark (*n*-type) contrasts and different brightness levels according to doping concentration in Si devices. It demonstrates that the secondary electron (SE) intensity is related to the dopant type and the doping concentration.

In this work, we measured 2D dopant profiles of the same multilayered *p-n* junction specimen with the LV-SEM and EH techniques. These techniques have their own strong and weak points. Therefore it is of great interest to study and improve performance of the techniques in order to make them more practical application in industry. Generally, 2D dopant profiling data were compared with SIMS depth profiles obtained from not real samples but non-patterned test samples. Comparison of 2D dopant profiling data performed by different techniques with the same sample is necessary to confirm and crosscheck the results. Furthermore, since these methods extract the 2D profiles depending on different physical properties of the *p-n* junction, it would be very important to precisely compare the obtained results.

MATERIALS AND METHODS

Preparation of Multilayered *p-n* Junction Specimens

To compare the detailed doping profiles, samples having a multilayered *p-n* junction structure were prepared by alternatively doping the phosphorus (P) and boron (B) atoms with dose of 2×10^{13} cm^{-2} using ion implantation energies varying from 50 keV to 1.2 MeV, followed by RTP anneal at 900°C for 15 sec. Implantation conditions were set to five alternating P and B doped layers, forming four *p-n* junctions. However, due to the lighter atomic weight of the boron (compared to phosphorous) it was diffused deeper into the substrate. Consequently, the number of doped layers has been changed, forming two P doped layers in sequence on the top of the specimen and three *p-n* junctions as indicated by M1, M2 and M3 in Fig. 1A.

2D Doping Profile Measurement by Low-voltage Scanning Electron Microscopy

Specimens for SEM observation were cleaved immediately before the loading in to the SEM in order to reduce the growth of native oxide layer and contaminations. All dopant contrast images were obtained using a field emission (FE)-SEM (S-4800; Hitachi, Hitachinaka, Japan) operated at accelerating voltage of 1 keV, emission current of 15~20 μA and working distance of 3~5 mm. The detector used for SE was the through the-lens upper detector. The dependence of the key parameters influencing dopant contrast as a function of accelerating voltage, emission current, working distance and others were reported by Venables et al. (1996) and El-Gomati et al. (2005). It was found that the yield of

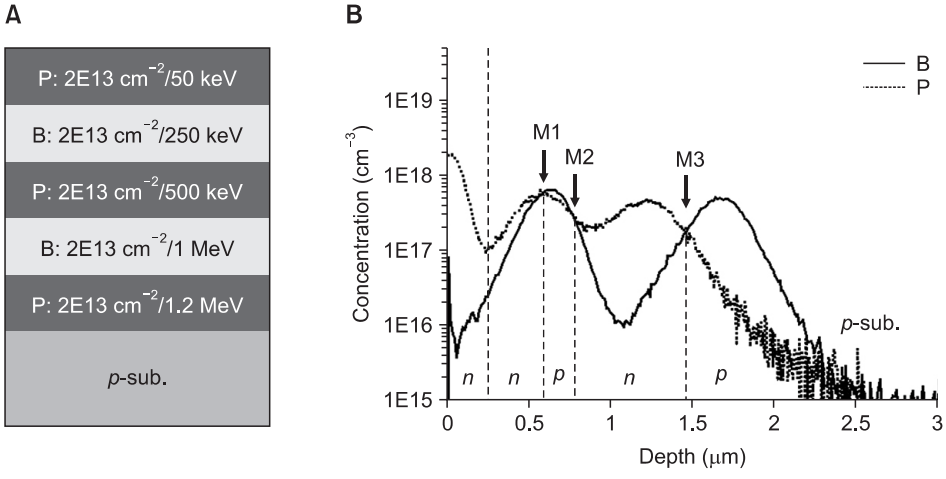

Fig. 1. Doping level distribution of the multilayered *p-n* junction test specimen. (A) The conditions of ion implantation process. (B) Secondary ion mass spectrometry depth profiles of P (----) and B (——) atoms in the test specimen. M1, M2 and M3 indicate the positions of the metallurgical *p-n* junctions. *p*-sub, *p*-type substrate.

SE from differently doped regions is mostly affected by the accelerating voltage. The best dopant contrast is obtained at the accelerating voltage of 1 kV and the contrast is gradually disappeared as accelerating voltage is above or below 1 kV.

2D Doping Profile Measurement by Electron Holography

Specimens for EH study were prepared by using the backside ion-milling method which was reported in detail elsewhere (Formanek & Bugiel, 2006a; Yoo et al., 2008). The basic procedure of this method is similar to the conventional cross-sectional TEM specimen preparation method. Briefly, during ion-milling thinning of the cross-sectional TEM specimen, Ar^+ ion beam was directed only from the substrate side to avoid formation of curtaining effects. Further, a window (usually 5×5 μm) was created using focused ion beam (FIB) technique to obtain the free space for the reference wave during EH measurements. Subsequently, surface damage, caused by Ga^+ ions during FIB milling, was removed by using low energy Ar^+ ion-milling for 3~5 min.

EH study was carried out using a FE-TEM (Tecnai G^2 F30 S-Twin; FEI, Hillsboro, OR, USA) equipped with a biprism and a 2 mega-pixel slow-scan charge coupled device camera for recording electron hologram. The biprism voltage, the spacing of the observed interference fringes and the field of view of the hologram were 40 V, 30 nm and 4 μm, respectively. Reconstructed phase images were obtained from the recorded holograms by performing Fourier transform and the subsequent inversed Fourier transform.

RESULTS

Fig. 1B shows the 1D SIMS profiles measured from our test specimen. The metallurgical *p-n* junction positions are indicated by M1, M2 and M3, respectively. Two P peaks are visible at the beginning of the profile (which is shown by the dashed line). Fig. 2 shows a schematic illustration of the ideal symmetric *p-n* junction and corresponding physical properties such as electric field, potential variation and charge distribution across the junction. It is well known that electrostatic field at the junction reaches to maximum value, and potential drops at the junction, forming a built-in potential, $V_{p\text{-}n}$. Generally in EH, the phase of electron waves passing through specimen containing the *p-n* junction region is modulated due to the variation of electrostatic potential across the junction as shown in Fig. 2. Apparently, the phase change is proportional to the potential drop at the junction. Therefore, the modulated phase of the recorded hologram causes to contrast difference in the reconstructed phase image, which reveals the specific doped regions (Twitchett et al., 2004).

LV-SEM Study

Detecting of SE contrast of doped semiconductors is very attractive in terms of easy performance and high resolution in modern SEMs. However there is no general mechanism explaining contrast phenomenon yet. From all suggested mechanisms, "metal-semiconductor contact" model seems to be more precise and explains the contrast mechanism taking in to account surface states of the specimen (El-Gomati et al., 2005). Other contrast models, such as "surface band bending" (Perovic et al., 1995) and "surface patch fields"

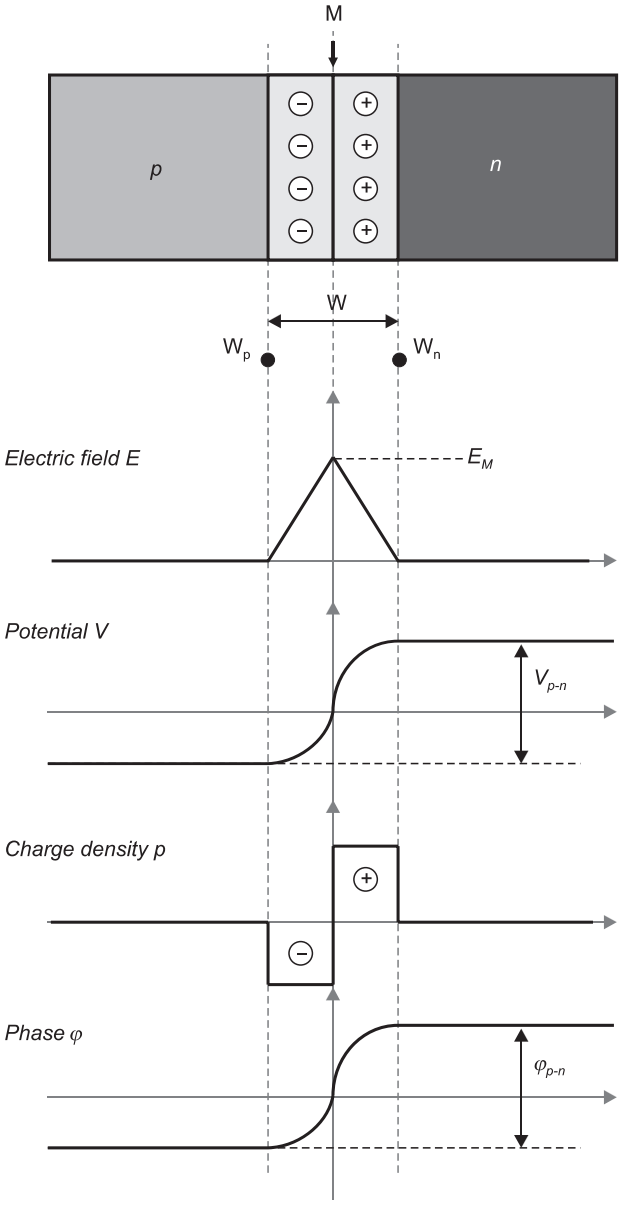

Fig. 2. Schematic illustrations of physical properties of the ideal symmetric *p-n* junction. It presents electric field, electrostatic potential, charge density and phase of the electron wave variation across the *p-n* junction.

(Sealy et al., 2000) explains the contrast mechanism on clean semiconductor surfaces, which is ideal case. According to the "metal-semiconductor contact" model, the thin carbon (C) layer generated on the specimen surface during SEM observation. As the work function of graphite carbon is greater than that of silicon, $\Phi_C > \Phi_{Si}$, Ohmic and Schottky contacts are formed on the *p* and *n* sides of the junction, respectively (El-Gomati et al., 2005). The existence of the Schottky barrier between *n*-type semiconductor and carbon will increase the potential barrier for SEs. As a result, the total SE yield from the *n*-type Si semiconductor will be reduced in comparison to that from the *p*-type one, hence showing a contrast difference between two differently doped regions. Typical LV-SEM image of differently doped silicon regions obtained at 1 keV is shown in Fig. 3A. Difference in dopant contrast between *p*- and *n*-doped regions is clearly distinguished as bright (boron implant) and dark (phosphorus implant) contrasts, respectively. Note that the contrast on the lightly doped *p*-type substrate region (V) is brighter than that of heavily doped *n*-type region (I and III) and darker than that of heavily doped *p*-type region (II and IV). The intensities of SE dopant contrast in LV-SEM image are as follows: C(*p*-doped)>C(*p*-substrate)>C(*n*-doped). Fig. 3B shows the SIMS depth profiles and the SE intensity profile extracted from the LV-SEM image presented in Fig. 3A, along the line X-Y. Three *p*-*n* junctions delineated by LV-SEM show very good agreement with the metallurgical *p*-*n* junctions measured by SIMS.

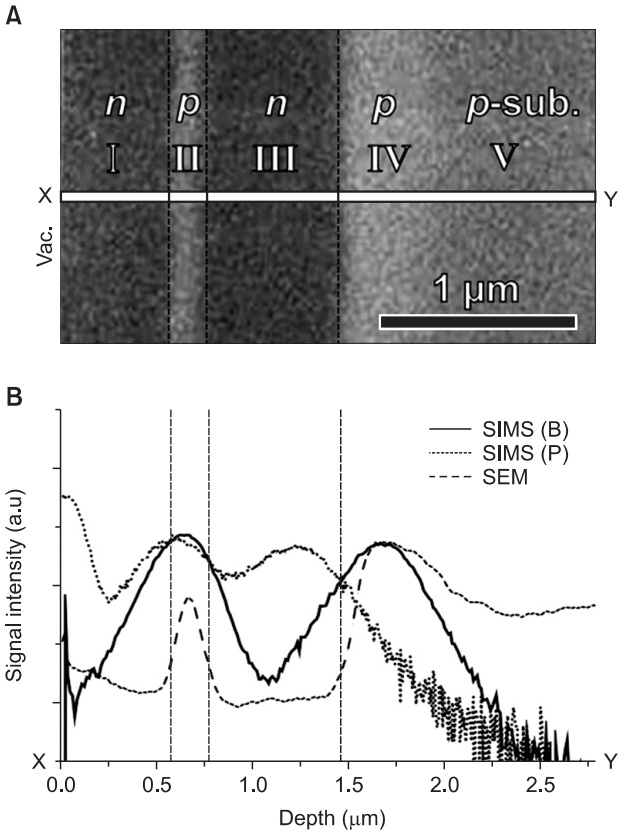

Fig. 3. (A) Scanning electron microscopy (SEM) micrograph shows the cross-section image of the multilayered *p*-*n* junction specimen at 1 keV. (B) Comparison of the secondary electron intensity profile extracted from SEM micrograph and secondary ion mass spectrometry (SIMS) depth profiles of B and P atoms. Note that the same junction depths were measured by both methods.

EH Study

EH does not directly provide the dopant concentration

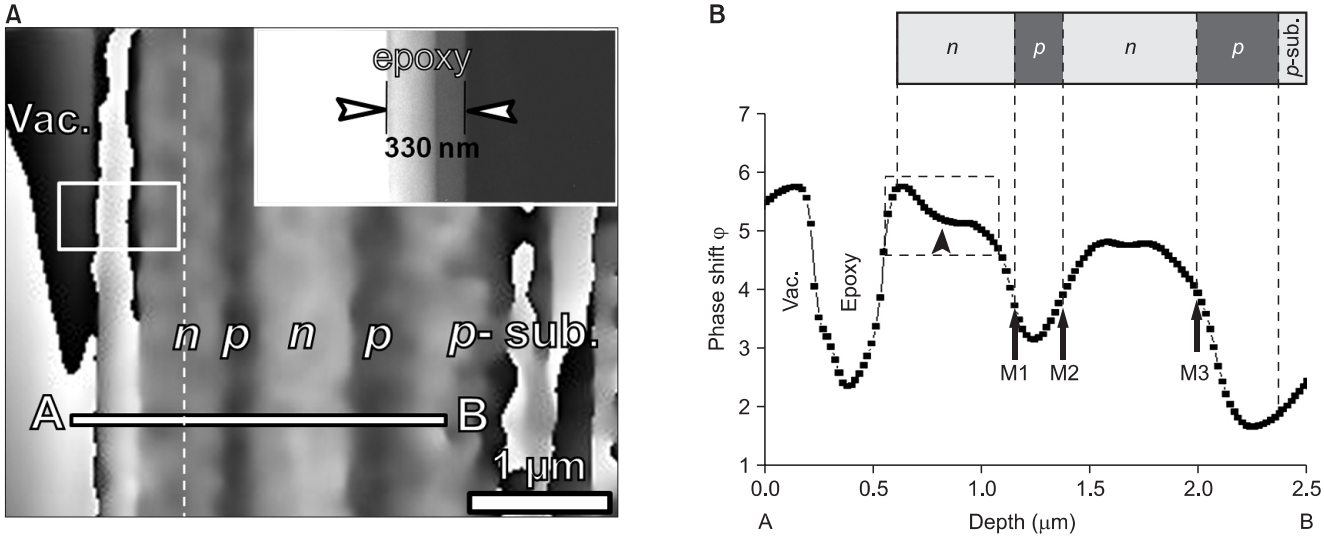

Fig. 4. Two-dimensional dopant profiling results by electron holography. (A) Reconstructed phase image obtained from the measured specimen. The inset of (A) shows the enlarged bright-field image of the box region in (A). (B) Phase profile measured along the line A-B in the phase image of (A). Vac., vacuum; *p*-sub., *p*-type substrate.

distribution or 2D dopant profile. In fact, it shows electrostatic potential distribution in the specimen. As phase shift is proportional to the potential drop at the junction (as shown in Fig. 2), the value of electrostatic potential can be extracted from the phase information measured from holography. The only way to relate the dopant concentration to electrostatic potential of holography is to calculate the potential using Poisson equation and Fermi-Dirac statistics (dopant concentration information from SIMS) and compare the two potential values.

Fig. 4 shows EH results obtained from the measured specimen. Fig. 4A shows a reconstructed phase image, where *p*- and *n*-doped regions in the specimen are visible with bright and dark contrasts, respectively. The bright-field image of the region near the surface is shown as the inset, where the remaining thin epoxy layer with the thickness of 330 nm is visible. Two *n*-doped layers in the top side of the specimen (as shown in Fig. 1A and B) are visible as one *n*-type layer with the 550 nm-thickness. Therefore, the reconstructed phase images reveal total four (*n*-*p*-*n*-*p*) doped layers and three *p*-*n* junctions on *p*-type substrate. The phase profile measured along the line A-B in the Fig. 4A is displayed in the Fig. 4B. The phase profile shows phase modulation due to the potential variation at the *p*-*n* junction, and each step in the profile corresponds to either *n*- or *p*-type regions of the specimen. The two *n*-type regions near the surface are distinguished with some difference of phase shift in the dashed box region in the Fig. 4B.

One of the main advantages of EH from other techniques is its high-spatial resolution. However, it is not always possible to obtain desired results. Because there are several problems associated with the TEM specimen for measuring hologram. Specimen preparation process for EH is required to be much more careful than for conventional TEM. The specimen has to maintain uniform thickness within the optimum range (usually 200~300 nm). Also, inactive layers existing on the specimen surface due to ion milling damage weaken doping contrasts. Low-kV milling is very good way to reduce the surface damage. Further, the presence of dynamic effects is another cause of difficulty in EH. In such a case, the phase of the electron wave does not reflect only doping contrasts in the specimen. To avoid diffraction contrast effect the specimen should be tilted to certain directions, which was studied by Formanek & Bugiel (2006b). Charging of the non-conductive parts in the specimen under the election beam generates another problem which hampers the real electrostatic potential of the specimen. These problems associated with specimen quality sometimes can greatly limit the practical application of EH.

DISCUSSION

Direct comparison of the results obtained from three analysis techniques are shown in Fig. 5. Fig. 5A and B depict reconstructed phase and SEM images, respectively. The positions of the metallurgical *p*-*n* junctions, M1, M2, M3 and depth of each doped layer are well matching in all results, which are indicated with dashed lines. At the same time, simulated potential profile for test specimen was compared with the profiles of the EH and SEM images as depicted in Fig. 5C. The simulation of potential profile was obtained by SILVACO (SILVACO, Inc., Santa Clara, CA, USA) simulation tool by inputting the process parameters for test specimen. Therefore it reflects the ideal case of potential distribution. On the other hand, as holographic phase change is proportional to the potential variation at the *p*-*n* junction (Venables & Maher, 1996), shape and distribution of the holographic phase profile should correspond to the potential variation. Indeed, both simulated potential profile and holographic phase profile show reasonable correspondence with each other as shown in Fig. 5C. Moreover, the intensity profile of

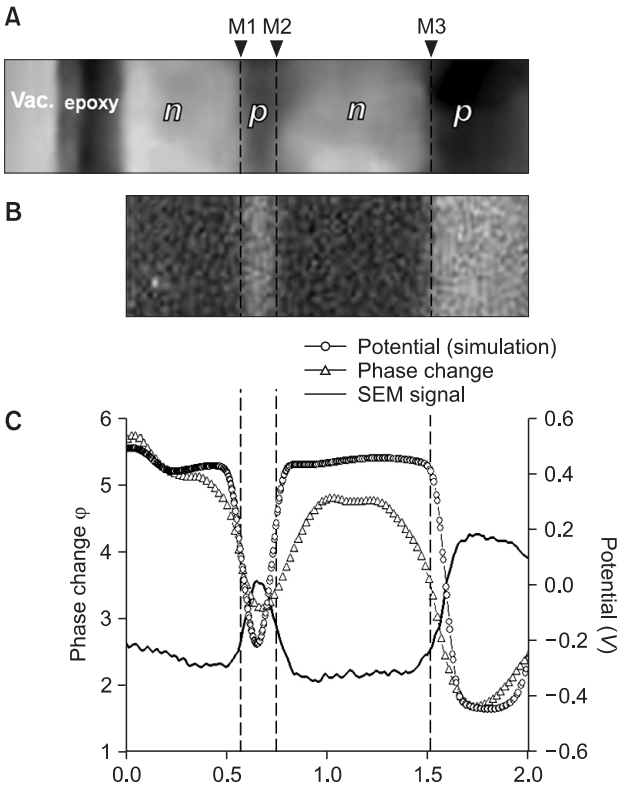

Fig. 5. Side-by-side comparison of two dimensional dopant profiling by (A) electron holography (EH), (B) low-voltage scanning electron microscopy (LV-SEM). (C) Comparison of EH and LV-SEM signal intensity and holographic phase profiles with simulated potential profile. Vac., vacuum.

the SE dopant contrast signal is also well matched with EH and simulation profiles.

CONCLUSIONS

In this study, we demonstrated the 2D dopant profiling of the multilayered *p-n* junction specimen with LV-SEM and EH methods. The side-by-side comparison of the results showed that junction depths and positions of the metallurgical *p-n* junctions are in good agreement with each other. From the obtained results we can conclude that two methods can be successfully employed to reveal the 2D dopant regions in semiconductor devices. EH can be used when high resolution and quantitative information is needed. However, it requires a long specimen preparation time and has several problems, such as inactive layer on the specimen surface and dynamic diffraction contribution to the phase image, whereas LV-SEM has advantages of a quick and easy process for obtaining the results with a simple sample preparation. Consequently, the combination of 2D dopant profiling techniques for analysis of the same specimen is very useful to obtain highly reliable information in nanometer scale devices.

REFERENCES

Bertrand G, Deleonibus S, Previtali B, Guegan G, Jehl X, Sanquer M, and Balestra F (2004) Towards the limits of conventional MOSFETs: case of sub 30 nm NMOS devices. *Solid-State Electron.* **48**, 505-509.

El-Gomati M, Zaggout F, Jayacody H, Tear S, and Wilson K (2005) Why is it possible to detect doped regions of semiconductors in low voltage SEM: a review and update. *Surf. Interface Anal.* **37**, 901-911.

Elliott S L, Broom R F, and Humphrey C J (2002) Dopant profiling with the scanning electron microscope: a study of Si. *J. Appl. Phys.* **91**, 9116-9122.

Eo H-J, Yang J-M, Park T-S, Lee J-P, Kim W, Park J-C, and Lee S-Y (2004) Chemical junction delineation of a specific site in Si devices. *J. Electron Microsc.* **53**, 277-280.

Formanek P and Bugiel E (2006a) Specimen preparation for electron holography of semiconductor devices. *Ultramicroscopy* **106**, 365-375.

Formanek P and Bugiel E (2006b) On specimen tilt for electron holography of semiconductor devices. *Ultramicroscopy* **106**, 292-300.

Morita S (2007) *Roadmap of Scanning Probe Microscopy* (Springer-Verlag, Berlin).

Perovic D D, Castell M R, Howie A, Lavoie C, Tiedje T, and Cole J S W (1995) Field-emission SEM imaging of compositional and doping layer semiconductor superlattices. *Ultramicorscopy* **58**, 104-113.

Rau W D, Schwander PF, Baumann H, Höppner W, and Ourmazd A (1999) Two-dimensional mapping of the electrostatic potential in transistors by electron holography. *Phys. Rev. Lett.* **82**, 2614-2617.

Sealy C P, Castell M R, and Wilshaw P R (2000) Mechanism for secondary electron dopant contrast in the SEM. *J. Electron. Microsc.* **49**, 311-321.

Shaislamov U, Yang J-M, Yoo J H, Seo H-S, Park K-J, Choi C-J, Hong T-E, and Yang B (2008) Two-dimensional dopant profiling in semiconductor devices by electron holography and chemical etching delineation techniques with the same specimen. *Microelectron. Reliab.* **48**, 1734-1736.

Tonomura A (1999) *Electron Holography* (Springer, Berlin).

Twitchett A C, Dunin-Borkowski R E, Hallifax R J, Broom R F, and Midgley P A (2004) Off-axis electron holography of electrostatic potentials in unbiased and reverse biased focused ion beam milled semiconductor devices. *J. Microsc.* **214**, 287-296.

Venables D and Maher D M (1996) Quantitative two-dimensional dopant profiles obtained directly from secondary electron images. *J. Vac. Sci. Technol. B* **14**, 421-425.

Völkl E, Allard L F, and Joy D C (1998) *Introduction to Electron Holography* (Plenum, New York).

Yoo J H, Yang J-M, Shaislamov U, Ahn C W, Hwang W-J, Park J K, Park C M, Hong S B, Kim J J, and Shindo D (2008) Electron holography study for two-dimensional dopant profile measurement with specimens prepared by backside ion milling. *J. Electron Microsc.* **57**, 13-18.

Zavyalov V V, McMurray J S, and Williams C C (1999) Scanning capacitance microscope methodology for quantitative analysis of p-n junctions. *J. Appl. Phys.* **85**, 7774-7783.